Conf-820839--9

DESIGN OF DOUBLY FOCUSING, TUNABLE (5 - 30 keV), WIDE-BANDPASS OPTICS MADE FROM LAYERED SYNTHETIC MICROSTRUCTURES

CONF-820839--9

DE83 015492

D. H. Bilderback,1 B. M. Lairson,1 T. W. Barbee, Jr.,2
G. E. Ice,3 and C. J. Sparks, Jr.,3

1 Cornell High Energy Synchrotron Source and
School of Applied and Engineering Physics
Cornell University, Ithaca, NY 14853, USA
2 Department of Materials Science and Engineering, Stanford University
Stanford, CA 94305, USA
3 Metals and Ceramics Division, Oak Ridge National Laboratory
Oak Ridge, TN 37830, USA

Abstract

Layered Synthetic Microstructures (LSMs) show great promise as focusing, high-throughput, hard x-ray monochromators. Experimental reflectivity vs. energy curves have been obtained on carbon-tungsten and carbon-molybdenum LSMs of up to 260 layers in thickness. Reflectivities for three flat LSMs with different bandpasses were 70% with $\Delta E/E = 5.4\%$, 66% with $\Delta E/E = 1.4\%$, and 19% with $\Delta E/E = 0.6\%$.

A new generation of variable bandwidth optics using two successive LSMs is proposed. The first element will be an LSM deposited on a substrate that can be water cooled as it intercepts direct radiation from a storage ring. It can be bent for vertical focusing. The bandpass can be adjusted by choosing interchangeable first elements from an assortment of LSM's with different bandpasses (for example, $\Delta E/E = 0.005$, 0.01, 0.02, 0.05, 0.1). The second LSM will consist of a multilayered structure with a 10% bandpass built onto a flexible substrate that can be bent for sagittal focusing. The result will

Paper presented at the International Conference on X-ray and VUV Synchrotron Radiation Instrumentation at DESY, Hamburg, W. Germany, August 9-13, 1982, and will be published as Conference Proceedings in Nuclear Instruments and Methods.

be double focusing optics with an adjustable energy bandpass that are tunable from 5 to 30 keV.

Introduction

It is feasible to construct new high-throughput hard x-ray monochromators from Layered Synthetic Microstructures (LSMs) that fully exploit the large energy range available from synchrotron radiation. LSMs consist of up to several hundred alternating layers of high and low density materials. Until now their greatest application has been in the soft x-ray domain as monochromators and analyzers.[1-4] This work reports on the feasibility of using tungsten-carbon and moly-carbon LSMs as wide bandpass ($\Delta E/E$ = 0.005 to 0.1) elements from 5 to 30 keV. We also discuss their focusing properties, and the potential of LSMs made from other materials.

Since the intensity of synchrotron radiation sources varies slowly with energy around the critical machine energy, a substantial gain in both intensity and power can generally be obtained by increasing the bandwidth of an optical system. For instance, doubling the bandwidth, $\Delta E/E$, of a monochromator may double its power output. Most monochromators are presently made from perfect cyrstals of germanium and silicon, with energy bandpasses of less than 10^{-3}. Such small bandwidths unduly restrict the monochromated power available for experiments where strict energy definition is not essential. For those experiments, power gains of 80 to 800 times over a perfect symmetric silicon (220) crystal are feasible, with bandpasses of 1% to 10%.[5] A total reflection mirror coupled with either an absorption filter or a transmission x-ray mirror have been demonstrated to perform ef-

ciently in the bandwidth domain of $\Delta E/E$ greater than 10%.[6] The bandwidth regime of $\Delta E/E$ of 0.005 to 0.1 can be covered with LSMs and can be utilized in a variety of experiments. The simultaneous coupling of wide bandpass optics with focusing in both horizontal and vertical directions will provide increased quantities of nearly monochromatic synchrotron radiation into areas of 1 mm^2 or less.

A wide variety of scientific experiments can effectively use the increased flux from wide bandpass optics. For instance, the bandwidth regime of $\Delta E/E$ between 1/2 and 1% is suitable for small molecule crystallography with crystal dimensions of up to 100 Å. Real time diffraction studies using both wide and small angle scattering methods can profitably trade higher incident beam intensities (from a 1% to 5% bandpass) for a corresponding loss of resolution in the diffraction pattern. The performance of a fluorescent microprobe would be enhanced by the gain in incident flu through a small aperature with little degradation due to the 1 to 10% spread in the excitation energy. These are just a few of the examples of the possible utility of wide bandpass optics.

Design Objectives

A wide bandpass monochromator can be described by its diffracting efficiency for x-ray radiation of different energies, its energy bandpass, its harmonic rejection capability, its ability to focus radiation to a point, and its stability under extreme heat and radiation loads.

(a) Diffraction Efficiency

Figure 1a schematically shows how nearly monochromatic x-rays can be selected from a synthetic crystal of layer spacing d by Bragg reflection. The

wavelength diffracted by a LSM is given by Bragg's law, $n\lambda = 2d \sin\theta \left(1 - \frac{S_o}{\sin^2\theta}\right)$ where n = 1,2,3, etc. for the various diffraction orders, λ = wavelength, S_o = average refractive index decrement and θ = angle of incidence. The term in parentheses corrects the Bragg equation for refraction by changing the angle of incidence, θ, the output in energy, $E(keV) = 12.4/\lambda$ (Å) may be varied over a considerable range. Figure 1b presents the desired response of the monochromator as a function of energy. In this example, the monochromator is set to diffract in first order (n = 1) at 10 keV. The desired reflectivity would by unity over a region ΔE about E_1 and the optics would provide some way of simply changing ΔE depending on the bandwidth desired for a given experiment. The reflectivity everywhere outside of the ΔE band would be zero (regions A and B. No monochromator, however, has the ideal response of Figure 1b and judgements must be made as to what reasonable low reflectivities are tolerable in regions A and B.

A LSM consists of alternating layers of two evaporated or sputtered materials A and B, of thickness dA and dB respectively deposited on a substrate. The structure may be periodic in a direction perpendicular to the planes, with a period d = dA+dB, or the structure may be a nonperiodic one where dA and dB vary as a function of depth perpendicular to the layered planes. The Fresnel equations can be used to calculate the reflection efficiency of synthetic multilayers as a function of energy. The reflectivity per layer pair is generally quite low for energies above the total reflection cutoff energy. However, the reflection amplitude of many layers may be made to add in phase giving rise to reflection efficiencies of 70 to 80% at x-ray energies. Figure 2 shows the calculated response of a tungsten-carbon LSM (d_W = 10 Å, d_C = 15.33 Å, $d = d_C + d_W$ = 25.33 Å) set to an angle of 30 milliradians. The peak reflectivity is 85%, and the bandpass $\Delta E/E$

(FWHM) is 3%. Figure 3 shows a tungsten-carbon LSM (d= 20 Å, $d_W = d_C$ = 10 Å, N = 100) set to 10.5 milliradians. The peak reflectivity is 85%, the bandpass is 2%.

Various computational approaches have been taken to solve Maxwell's equations for materials having an index of refraction that varies as a function of depth. In one approach, the reflection amplitude is calculated for the interface between the bottom layer and the substrate. A recursion relationship is then used to calculate the reflection amplitude at the interface one layer above it. This process is repeated until the reflection amplitude for the top layer has been obtained (which includes the effects of all the layers beneath it).[7,8] Another approach has been to solve the problem with matrix methods commonly used in optical multilayer calculations.[9] All of these methods can be used to find exact solutions that apply to both periodic and nonperiodic reflectors whose layers can model arbitrary gradients in the index of refraction. The calculations presented in this work were made using a Fortran computer program which adopted the recursion method, as developed by Parratt.[8]

To begin the computation of reflectivity, materials A and B must be chosen. One material is generally of high electron density and the other of low electron density to enhance the change in the real part of the index of refraction from material A to material B. The number of layer pairs, N, and the thickness of the layer pair, d, are the next basic variables to be optimized for a design to satisfactorily cover a given range of energies with a specified bandpass.

The refractive index, n, can be expressed as $n = 1 - \delta - i\beta$ for each material, where

$$\delta = \frac{1}{2\pi} \left(\frac{e^2}{mc^2} \right) \left(\frac{N_0 \rho}{A} \right) [z + \Delta f'] \lambda^2$$

$$\beta = \frac{\lambda \mu}{4\pi}$$

The term δ is of the order 10^{-5} and is the decrement of the index of refraction. e^2/mc^2 is the classical radius of the electron, $\frac{N_o \rho}{A}$ the number of atoms per unit volume, and λ the wavelength. The term $[z + \Delta f']$ is the real part of the scattering factor for the media being discussed, and includes the dispersion term $\Delta f'$, which is small except near absorption edges. The imaginary part of the index of refraction, β , gives rise to absorption and is a function of the linear absorption coefficient μ . Values for $\Delta f'$ and μ for different materials can be found in references 10 and 11, respectively. The square of the index of refraction, n, is equal to the complex dielectric constant for the medium. Values for the index of refraction for various materials are fairly well known in the hard x-ray regime, but are less certain for soft x-rays.

(b) Energy Bandpass

The bandwidth of an LSM is controlled by the number of layer pairs sampled by the x-rays and by variations in the d-spacing of the microstructure with depth. The bandwidth is related to the number of layers participating in the reflection process through the Sherrer equation[12] which can be expressed in energy as $\Delta E/E = 1.8\ N_e$; N_e = effective number of layers participating in the first order diffraction peak. It is well known that the x-ray diffraction lines from a polycrystalline powder sample can be broadened by having a small particle size. The bandwidth of the LSM can be viewed as line broadening from small particles whose size is equal to the total layer spacing, $N_e d$.

The penetration depth (and hence the number of layers sampled) is controlled by the reflecting power per layer pair and the absorption coefficients of materials A and B, for a given angle of incidence and d-spacing. Thus, large bandpass LSM's can best be fabricated by using a very high z

material for one component. Optics with a small bandpass, on the other hand, are better made with lower z elements so that constructive interference from many more layers can take place, narrowing the widths of the Bragg peaks.

Another method of altering the bandwidth of an LSM is to vary the ratio dA/dB and/or the d-spacing as a function of depth in the structure.[13,14] Spiller calculated that the integrated reflectivity of a 91 layer tungsten-carbon structure could be increased by almost a factor of 2 if the layers were appropriately graded.[13] In this instance, the calculated bandpass could be increased from 3% to 10%, while the peak reflectivity fell from 75% to 46%. Nagel, Barbee, Jr., and Gilfrich have examined LSM's in which the d-spacing varied as a function of depth, and have found good agreement between theoretically predicted and observed reflectivities.[14] We have calculated reflectivity vs. energy curves for enhanced bandwidth LSMs; four of these curves are shown in Figure 4 (all had 135 layers and incidence angles of 38.7 mr). Curve (a) is for a W-C LSM with $d = 20$ Å and $d_W/d = 0.3$. Curve (b) is for the same structure with $d_W/d = 0.5$. Curves (c) and (d) show reflectivity for LSMs in which d_W/d and the d-spacing vary with depth. In (c), the d-spacing increases from 19.5 Å for the top layer to 20.3 Å for the bottom, with the ratio d_W/d increasing from 0.2 to 0.5. In (d), the d-spacing varies from 19.2 Å to 20.8 Å and the ratio d_W/d goes from 0.2 to 0.5 from the top layer to the bottom layer. Curves (c) and (d) have bandpasses of 3% and 5.7%; they show increases in integrated reflectivity over curve (b) of 30% and 55% respectively.

(c) Harmonic rejection

A particularly troublesome problem for most monochromators (crystals,

gratings, LSMs, etc.) is that they generally have nonzero reflectivity at multiples of the fundamental monochromator energy (i.e. 2E1, 3E1, etc., corresponding to n = 2,3,4,...). In the case of a perfect double crystal monochromator, the intensity of the harmonics can be reduced by two to three orders of magnitude by detuning the first crystal with respect to the second by up to several seconds of arc.[16,17] Alternatively, a total reflection mirror can be placed either before or after the monochromating element to reflect the fundamental but not the harmonics.[18]

The harmonic rejection capabilities of a periodic LSM are controlled by the way in which the index of refraction changes within a layer pair. An angle-dependent one dimensional structure factor can be defined for a single layer of thickness d, which is the Fourier transform of the index of refraction taken over the thickness of the layer. The reflectivity of a periodic LSM is proportional to the square of this structure factor. If the index of refraction vs. depth is a step function, representing an LSM having perfectly sharp interfaces between materials A and B with dA=dB, then all even order reflections (n = 2,4,6,...) will be forbidden; only odd order reflections will be allowed. If the interfaces between materials A and B are not sharp, i.e., if the index of refraction varies continuously at the interfaces, the higher order reflections will be somewhat suppressed.[7]

If the index of refraction varies sinusoidally with depth, then only the fundamental will be present; all higher order reflections will be completely suppressed.[7,9,19,20] Figure 5 shows the reflectivity vs. energy of a 20 Å period W-C LSM, set to an angle of 38.7 mr. The index of refraction was modeled to vary as a function of depth according to

$$n(z) = \left(\frac{n_A+n_B}{2}\right) + \left(\frac{n_A-n_B}{2}\right) \sin\left(\frac{2\pi z}{d}\right)$$

by dividing each period of thickness d into 40 sublayers and calculating reflectivity using the recursion relation. Clearly, modulating n (z) with a sine wave dependence is of great benefit in supressing the diffraction orders beyond the fundamental or first order reflection.

(d) Focusing ability

For a LSM monochromator to achieve optimum sagittal focusing, the reflection must be specular with respect to the figured surface of the optical element. Since mosaic crystals introduce an additional divergence due to their mosaic spread, it is difficult to focus all the radiation to very small spot sizes with the several meter focal lengths employed at synchrotron radiation sources.

For focusing over a range of energies, the figure of the optical element must be adjustable. Departures from the ideal figure, as manifested in slope errors, increase the size of the focused image. ~~reduce the effectiveness of the focusing, particularly from slope errors~~. Generally, the tolerable slope errors can be no larger than 2 to 10 seconds of arc depending on the magnification of the optics and the quality of the focused image expected.

(e) Stability

The monochromator must not change over time when exposed to synchrotron radiation. Not only is mechanical stability important in the supporting structure, but the optical element itself must withstand the severe thermal gradients and radiation doses that are received by the element exposed to direct synchrotron radiation. LSMs have been shown to be stable in a white synchrotron radiation beam for continuous periods of up to several months with no significant deterioration of their ability to diffract x-rays.[21]

Experimental Reflectivity Measurements

The performance of three LSMs synthesized by T. Barbee, Jr. of Stanford

were measured at CHESS as a function of energy and angle of incidence. Figure 6 shows the experimental arrangement for the reflectivity measurement. Slits S1 and S2 provided a beam to the LSM with less than 2 arc second divergence. Another horizontal slit (not shown) limited the beam to a 1 mm horizontal width. With these vertical slits, the (220) silicon channel cut monochromator on the A2 station had an energy resolution of less than 1 ev at 8 keV and could be scanned from 7 to 40 keV. The receiving aperature on the scintillation counter, C, subtended 1 milliradian. The 10 micron high beam incident at a grazing angle of 35 milliradians illuminated a 0.3 mm strip on the LSM. A counter in position (1) could count the direct beam or could be positioned at (2) to receive the reflected beam. The ratio of the two measurements gave directly the experimental reflectivity. Parameters were adjusted so that the incident count rate did not exceed 25,000 counts per second in the region of the first order diffraction peak, but this was increased to 60,000 counts per second in the region where $R < 0.01$ (with dead time corrections of up to 8%). (The incident beam in fact was measured only on every fifth to tenth data point; Compton scattering from a 25 micron thick mylar sheet was monitored ahead of S2 for the intervening points). The monochromator was detuned through a weak link to minimize harmonic throughput and stabilized with a feedback circuit.[17] A single channel analyzer then removed any contribution from harmonics and reduced pulse pileup.

Figure 7 shows the measured reflectivity for a 21.4 Å spacing LSM with 110 layers each of carbon and tungsten. Most notable is the 66% peak reflectivity with a bandwidth $\Delta E/E$ of 1.4% FWMH at 8.55 keV. The first harmonic reflectivity at 16.86 keV is down by a factor of 1200 over the fundamental, making this LSM a very efficient wide bandpass element with good harmonic rejection. Interference oscillations from the various layers are clearly

resolved on the tails of the first order diffraction peak. Figure 8 shows the experimental response of a 55 Å molybdenum-carbon LSM. The 30 layers yield a bandwidth of 5.4% at 8.1 keV. Greater than 70% peak reflectivity is observed for the fundamental diffraction peak. A strong second order peak at 15.6 keV is observed, which could be suppressed in future designs.

Several additional plots were made of the 55 Å LSM using an energy dispersive technique described elsewhere.[22] Figure 9 shows that a 5.3% bandwidth at 22.5 keV was observed with a peak reflection efficiency of 70%. The first harmonic bandwidth was much smaller, 2.1% at 43 keV.

Figure 10 is of a 260 layer tungsten-carbon LSM with a d-spacing of 15 Å and an angle of incidence of 51.7 milliradians. It has an experimentally observed bandwidth of 0.6% and a peak reflectivity of 19%.

X-Ray Topographs

Several topographic pictures were taken from various microstructures, Figure 11. The experimental arrangement of Figure 6 was retained except that slit 3 and the counter were removed and a sheet of Kodak type M film was placed 1.3 meters downstream from the LSM. A diffraction pattern from slit S2 was clearly recorded on the film, Figure 11a, for 8.041 keV x-rays. A shift in the diffraction pattern of 1/5th of the vertical separation between maxima of the diffraction pattern would be discernable. This translates to an angular sensitivity on the film of two arc seconds. Thus we could detect a change in slope on the LSM by half of this amount or one second of arc. The Bragg reflected image, Figure 11b, shows considerable structure corresponding to slope variations of about 10 arc seconds on the LSM surface, and as a result, the inteference pattern is lost. This angular spread can arise from having an imperfect substrate and/or multilayer coating. Two other pictures were

taken to ascertain the quality of the substrate beneath the multilayers. Figure 11b is a total reflection topograph taken of a typical commercial (111) silicon wafer used for multilayer substrates. Figure 11d shows the corresponding total reflection topograph taken at the same energy and the same angle of incidence. It is clear from comparing 11c with 11d that the vertical spread in the reflected images are virtually identical, hence, the slope errors are the same. We conclude that the multilayer coating basically mimics the undulations of the substrate. This suggests that much higher quality substrates are needed before imperfections from the layered structure itself can be made prominent.

Sagittal Focusing with Multilayers

A simple two-dimensional focusing monochromator with a wide bandpass can be constructed from LSMs by deposition on a doubly curved substrate. This device with fixed radii will focus at only one energy and one magnification. A more versatile focusing and energy tunable system would have an LSM singly curved in the scattering plane to focus the vertical divergence. This would be followed be a cylindrically or conically curved LSM which sagittally focuses the horizontal beam divergence as shown in Figure 12. The use of two multilayers in the (1, -1) nondispersive geometry has the advantage of keeping the scattered beam fixed in space. These shapes can be dynamically bent following a focusing method that has been successfully applied to perfect crystals.[23-25] We envision the substrate for the multilayers to be reinforced against anticlastic bending (for radii of 5 to 50 cm) as shown in Figure 12. A LSM 10 cm long located 10 m from the source with a 15 mr Bragg angle can collect 30 times as much radiation in sagittal focusing as compared with meridional focusing. For a d-spacing of 20 Å and a magnification of one, the horizontal divergence

which can be collected by a 10cm long LSM with a focal length of 10 m, is 87 mr/E(keV). At magnification 1/3, 37 mr/E(keV) can be intercepted by the same LSM.

A Monte Carlo ray tracing program was used to test the focusing and transmission properties of a nondispersive multilayer pair as shown in Figure 12. Ray tracing for LSMs can be treated just as diffraction from crystals where the $\Delta E/E$ is derived from the Darwin width. A realistic source, with a Gaussian intensity distribution and with adjustable dimensions and divergences, was used for the calculation. A uniform horizontal intensity distribution was assumed. Bragg reflections from the ~~second of the~~ two LSMs occurred over a range of Bragg angles determined by the bandwidth, $\Delta E/E$, ~~of the second LSM~~. The mosaic spread of the LSM was assumed negligible. The sagittal focusing LSM was taken to have a bandwidth of 0.1, while the bandwidth of the vertically focusing LSM was varied between 0.005 and 0.1. We have assumed a d-spacing of 20 Å for both LSMs. Results for selected cases are tabulated in Table 1 for the source size expected at the National Synchrotron Light Source (NSLS). The image size for CHESS can simply be obtained by scaling the results by the ratio of the actual CHESS source size to the expected NSLS source size. Sagittal focusing of the horizontal divergence always mixes the horizontal into the vertical divergence causing additional vertical angular spread at the sample. The magnitude of this effect is displayed in the last two columns of Table 1.

Transmission, which is defined as the radiation which the second LSM passes relative to that passed by the first LSM, is excellent because of the wide energy bandpass of the second LSM. In most cases, transmission is nearly the same as that through two flat multilayers with the same peak reflectivity and bandwidths. Therefore, intensity gains over the usual perfect crystal optics will scale as the ratio of bandpasses (80 to 800 times more intensity for a 1 to 10% LSM when compared to 220 silicon). This assumes the crystal optics

accept no more horizontal milliradians than the LSM and that the LSM has the same peak reflectivity as the single crystals.

Conclusion

We have completed a feasiblity study of the properties of layered synthetic microstructures as hard x-ray monochromators. The high peak reflectivities and large bandwidths offer the opportunity to create very powerful focusing optics for synchrotron radiation. Our next step is to fabricate wide bandpass LSMs on bendable substrates with areas greater than 100 cm^2.

Acknowledgements

We are indebted to D. Mancini for his help on the topographical information presented. This work was supported by Grant No. DMR81-12822[illegible] from the National Science Foundation through CHESS, the Cornell High Energy Synchrotron Source, and the School of Applied and Engineering Physics at Cornell University and by the Materials Sciences Division, U. S. Department of Energy, under contract W-7405-eng-26 with the Union Carbide Corporation. The work by T. W. Barbee, Jr., at Stanford University was supported by the U. S. Department of Energy through the Lawrence Livermore National Laboratory.

Table I. Multilayer ray tracing results showing how image size and vertical convergence depend on various optical parameters. A one sigma source size of 0.4 mm horizontal by 0.125 mm vertical with a one sigma vertical divergence of 0.059 milliradians is assumed (projected NSLS source size). The model LSM d-spacing is 20 A, with a 2nd element bandpass of 10% for a nominal x-ray energy of 20 keV. Transmission is better than 97% of the transmission for two flat LSMs for all the cases shown.

dE/E (first multilayer)	Mag	Horizontal divergence (mrad)	Image size (mm)		Vertical 1 σ convergence (rad)
			hor (1 σ)	vert (1 σ)	
0.10	1	2	0.40	0.15	5.8×10^{-5}
0.10	1	4	0.42	0.16	9.3×10^{-5}
0.10	1	6	0.51	0.18	1.7×10^{-4}
0.10	1	8	1.06	0.25	5.7×10^{-4}
0.10	1/3	4	0.15	0.062	1.7×10^{-4}
0.10	2	4	0.88	0.32	2.0×10^{-5}
0.005	1	4	0.43	0.18	9.3×10^{-5}
0.01	1	4	0.42	0.16	9.1×10^{-5}
0.05	1	4	0.42	0.16	9.3×10^{-5}

Figure Captions

Fig. 1a White radiation emerges from the synchrotron source and passes through a slit. Nearly monochromatic x-rays of energy E can be selected ~~from~~ with a synthetic crystal of layer spacing d by Bragg reflection.

1b Ideal response of an x-ray monochromator as a function of energy. The monochromator has unity reflectivity for a range of energies, E, around the energy E_1 (here set to 10 keV) and zero elsewhere. The energies $2E_1$ and $3E_1$ are the positions of the first and second harmonics; most monochromators have difficulty completely rejecting harmonic contaminents.

Fig. 2 Calculated reflectivity vs. energy of tungsten-carbon LSM with sharp interfaces (d=25.33 A, d_W= 10 A, d_C= 15.33 A, N = 100 layers, θ= 30 mr). The fundamental has a peak reflectivity of 85% at 8 keV, with a bandpass of 3%.

Fig. 3 Calculated reflectivity vs. energy of a tungsten-carbon LSM (d = 20 Å, N = 100 layers, $d_W = d_C$= 10 Å, θ = 10.5 mr). The fundamental has a peak reflectivity of 85%, and a bandpass of 2%.

Fig. 4 Calculated reflectivity vs. energy of four 135 layer, tungsten-carbon LSMs in which the ratio d_W/d (the thickness of the tungsten to the total layer thickness) and the d-spacing vary as a function of depth. Parameters are:

Curve (a): $d_W/d \doteq 0.3$, d = 20 Å, θ = 38.7 mr

Curve (b): d_W/d = 0.5, d = 20 Å, θ = 38.7 mr ← insert

Curve (c): d_W/d increases from 0.2 to 0.5 and the d-spacing

The shift in energy from curve (a) is due to a change in the average index of refraction.

grows from 19.5 to 20.3 Å from the top to the bottom layer.

Curve (d): d_W / d varies from 0.2 to 0.5, and the d-spacing increases from 19.2 to 20.8, from top to bottom.

Fig. 5 Calculated reflectivity vs. energy for a tungsten-carbon LSM. The index of refraction is modeled to vary sinusoidally with depth in a 20 Å period by varying the relative proportions of tungsten and carbon. The sinusoidal variation in the index of refraction causes all harmonics to be completely suppressed. (N = 100 layers, θ =38.7 mr). The fundamental has a peak reflectivity of 70% and a bandpass of 1.8 %.

Fig. 6 Synchrotron radiation was made monochromatic by a silicon (220) monolith and collimated to a 2 arc second vertical divergence by S1 and S2. The beam intensity ahead of S2 was monitored by measuring the Compton scattering from a 25 micron thick mylar sheet. A 0.4 mm high slit, S3, just ahead of a scintillation counter, C, was used to scan the direct or reflected images.

Fig. 7 Measured reflectivity vs. energy of a tungsten-carbon LSM #80-010 (d = 21.4 Å, N =100, d_W = 8.56 Å, d_C = 12.84 Å, θ = 34.9 mr). The fundamental has a peak reflectivity of 66%, and an energy bandpass of 1.4%.

Fig. 8 Measured reflectivity vs. energy of a molybdenum-carbon LSM #80-071 (d = 56 Å, N = 30, d_W = 26 Å, d_C = 30 Å, θ = 15 mr). The fundamental has a peak reflectivity of 72%, and an energy bandpass of 5.4%.

Fig. 9 Measured reflectivity vs. energy of a molybdenum-carbon LSM #80-071 ($d = 56$ Å, $N = 30$, $d_{Mo} = 26$ Å, $d_C = 30$ Å, $\theta = 5.15$ mr). The fundamental shows a peak reflectivity of 70%, and a bandpass of 5.3% The data was taken with a Si(Li) detector and with a conventional tungsten x-ray tube.

Fig. 10 Measured reflectivity vs. energy of a tungsten-carbon LSM #82-047. ($d = 15$ Å, $\theta = 51.7$ mr, $N = 260$ layers, $d_W = 67$ Å $d_C = 8.3$Å). The fundamental has a peak reflectivity of 19% and a bandpass of $\Delta E/E$ of 0.6%.

Fig. 11 Topographic comparison of a Layered Synthetic Microstructure with a bare silicon wafer substrate. a) Direct beam diffraction pattern from slit S2 of Figure 4 for 8.04 keV x-rays. b) Bragg reflected image of (a) by a tungsten-carbon LSM #82-010 ($d=21.4$ Å, $N = 110$, $\theta = 34.9$ mr). c) Total reflection topograph of (a) by a commercial (111) silicon wafer substrate at a 3.5 mr grazing angle. d) Total reflection topograph of (a) by LSM #82-010 at a 3.5 mr grazing angle.

Fig. 12 Proposed doubly focusing multilayer optics scheme that can be tuned in energy from 5 to 30 keV. The first element controls the bandwidth of the entire optics. It will consist of interchangeable LSMs of different bandpasses, (for instance, 0.5%, 1.0%, 2.0%,5.0%,10.0%) and can be bent for vertical focusing. The second element has a 10% bandwidth, can be bent for focusing in the horizontal plane, and is reinforced with ribs to minimize anticlastic bending effects.

References

1. B. L. Henke, AIP Conf. Proc. No. 75 on Low Energy X-Ray Diagnostics (1981) 85.
2. E. Spiller, AIP Conf. Proc. No. 75 on Low Energy X-Ray Diagnostics (1981) 124.
3. T. W. Barbee, Jr., AIP Conf. Proc. No. 75 on Low Energy X-Ray Diagnostics (1981) 131.
4. G. L. Stradling, T. W. Barbee, Jr., B. L. Henke, E. M. Campbell, and W. C. Mead, AIP Conf. Proc. No. 75 on Low Energy X-Ray Diagnostics (1981) 292.
5. D. H. Bilderback, Nucl. Instrum. Methods 195 (1982) 67.
6. B. M. Lairson and D. H. Bilderback, Nucl. Instrum. Methods 195 (1982) 79.
7. J. H. Underwood and T. W. Barbee, Jr., AIP Conf. Proc. No. 75 on Low Energy X-Ray Diagnostics (1981) 170.
8. L. G. Parratt, Phys. Rev. 95 (1954) 359.
9. A. E. Rosenbluth and J. M. Forsyth, AIP Conf. Proc. No. 75 on Low Energy X-Ray Diagnostics (1981) 280.
10. D. Cromer and D. Liberman, J. Chem. Phys. 53 (1970) 1891.
11. J. H. Hubbel, Atomic Data 3 (1971) 241.
12. B. E. Warren, X-Ray Diffraction (Addison-Wesley Publishing Co., Inc.,,969) chptr. 13.
13. E. Spiller, Appl. Phys. Lett., 20 (1972) 365.
14. D. J. Nagel, T. W. Barbee, Jr., and J. V. Gilfrich, Proc. Soc. Photo. Opt. Instrum. Engr. 315 (1981) 110.
15. E. Spiller, private communication.
16. M. Hart and A. R. D. Rodrigues , J. Appl. Crystallogr. II (1978) 248.
17. D. Mills and V. Pollock, Rev. Sci. Instrum. 51 (1980) 1664.
18. D. H. Bilderback, Proc. Soc. Photo. Opt. Instrum. Engr. 315 (1981) 90.
19. B. L. Henke, AIP Conf. Proc. No. 75 on Low Energy X-Ray Diagnostics (1981) 146.
20. A. M. Saxena and B. P. Schoenborn, Acta Crystallogr. Sec. A: 33 (1977) 805.

21. T. W. Barbee, Jr. and W. K. Warburton, private communication.

22. D. H. Bilderback and S. Hubbard, Nucl. Instrum. Methods 195 (1982) 85.

23. C. J. Sparks, Jr., G. E. Ice, J. Wong, and B. W. Batterman, Nucl. Instrum. Methods 195 (1982) 73.

24. C. J. Sparks, Jr., G. E.Ice, M. Willey,and J. Heck, to be published in Rev. Sci. Instrum.

25. G. E. Ice and C. J. Sparks, Jr., to be published in J. Opt. Soc. Am.

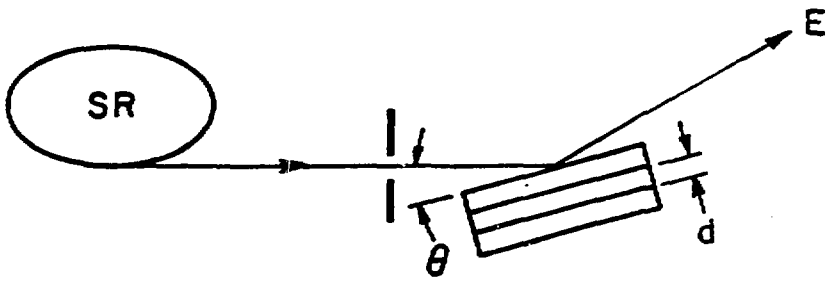

(a)

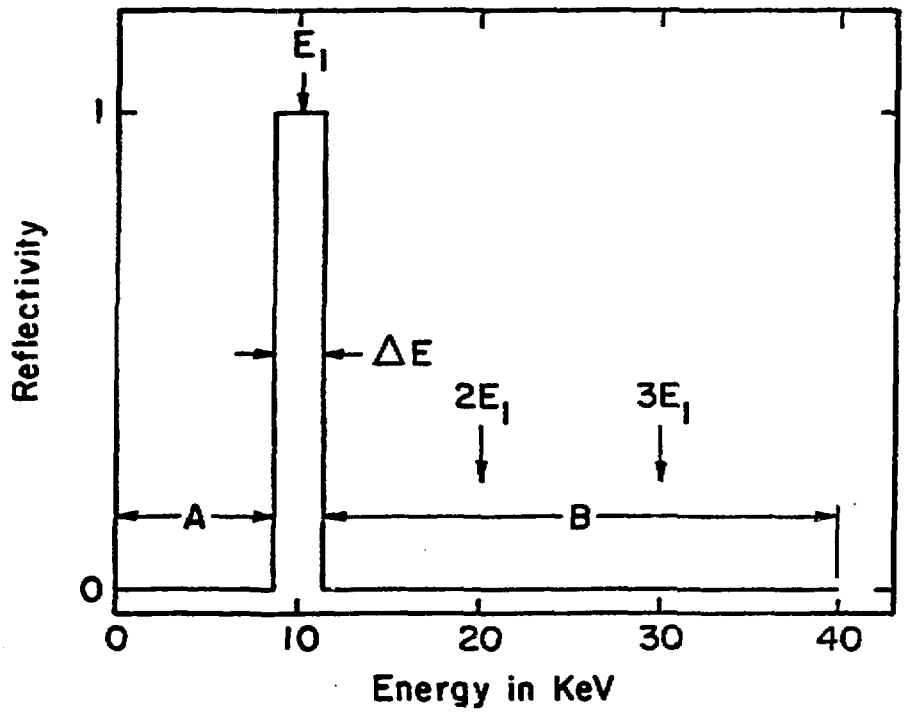

(b)

2120682

Figure 1.

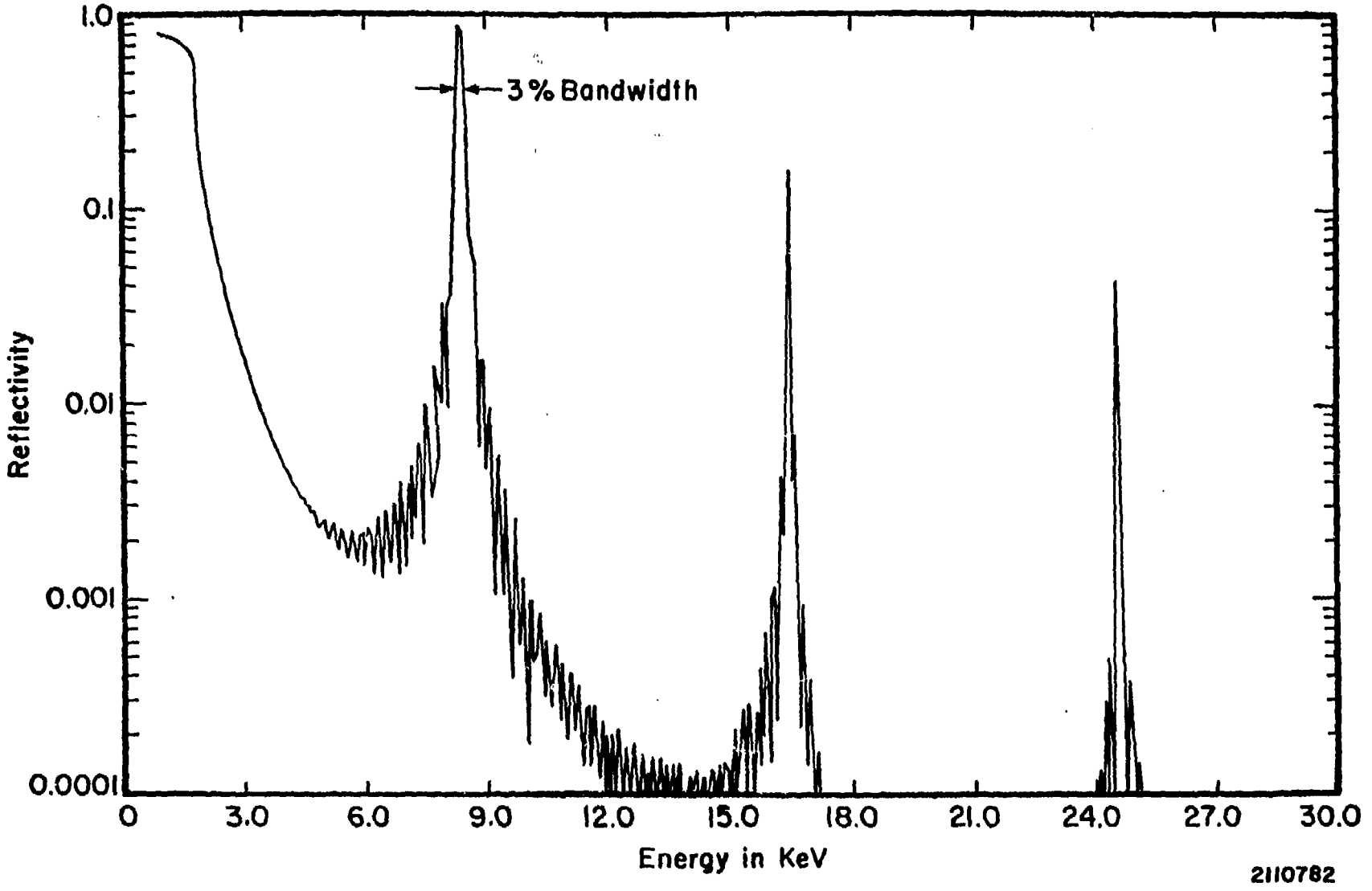
1.0
0.1
0.01
0.001
0.0001
Reflectivity
3% Bandwidth
0
3.0
6.0
9.0
12.0
15.0
18.0
21.0
24.0
27.0
30.0
Energy in KeV
2110782

Figure 2

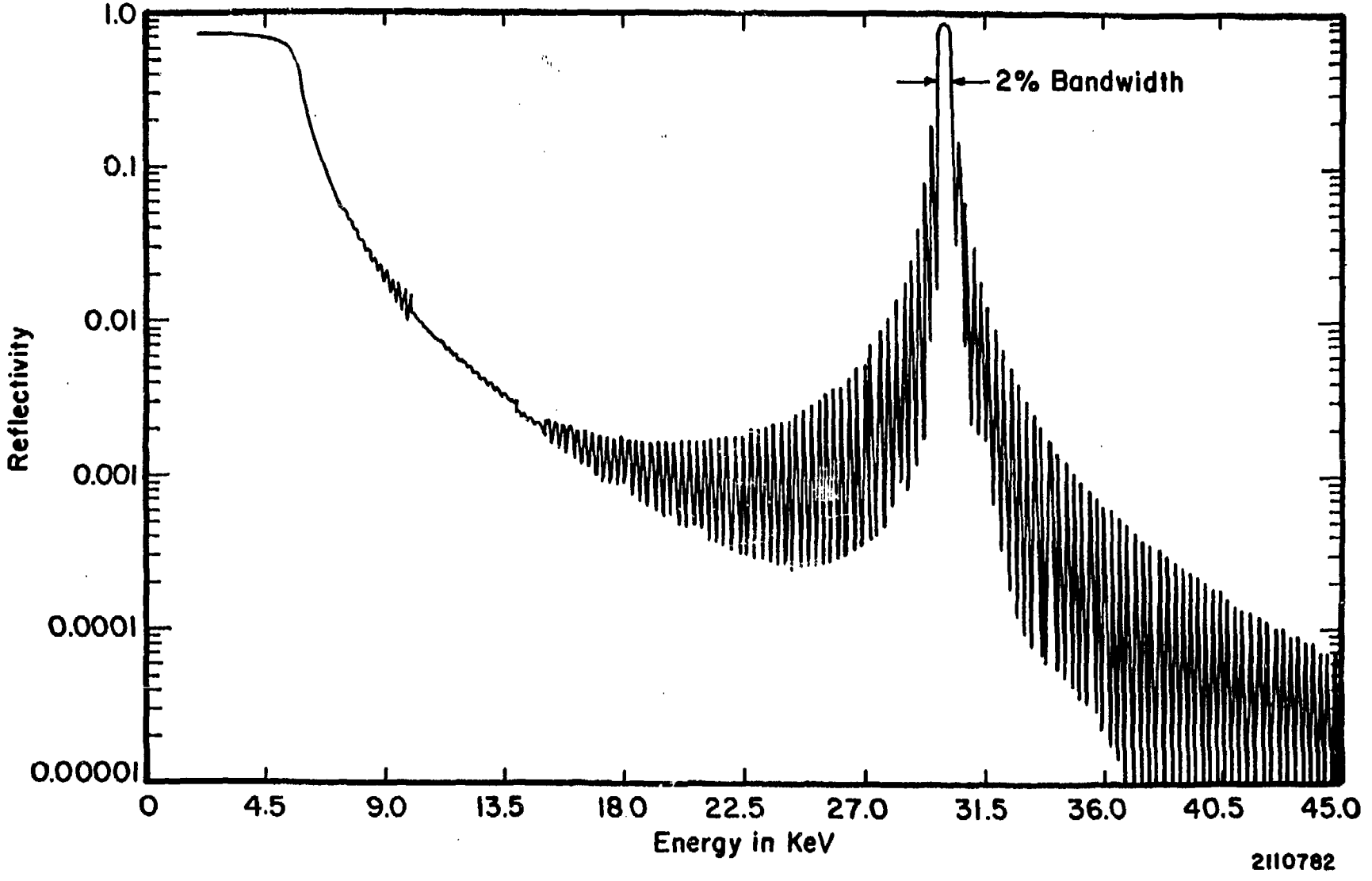
1.0
0.1
0.01
0.001
0.0001
0.00001
Reflectivity
2% Bandwidth
0
4.5
9.0
13.5
18.0
22.5
27.0
31.5
36.0
40.5
45.0
Energy in KeV
2110782

Figure 3

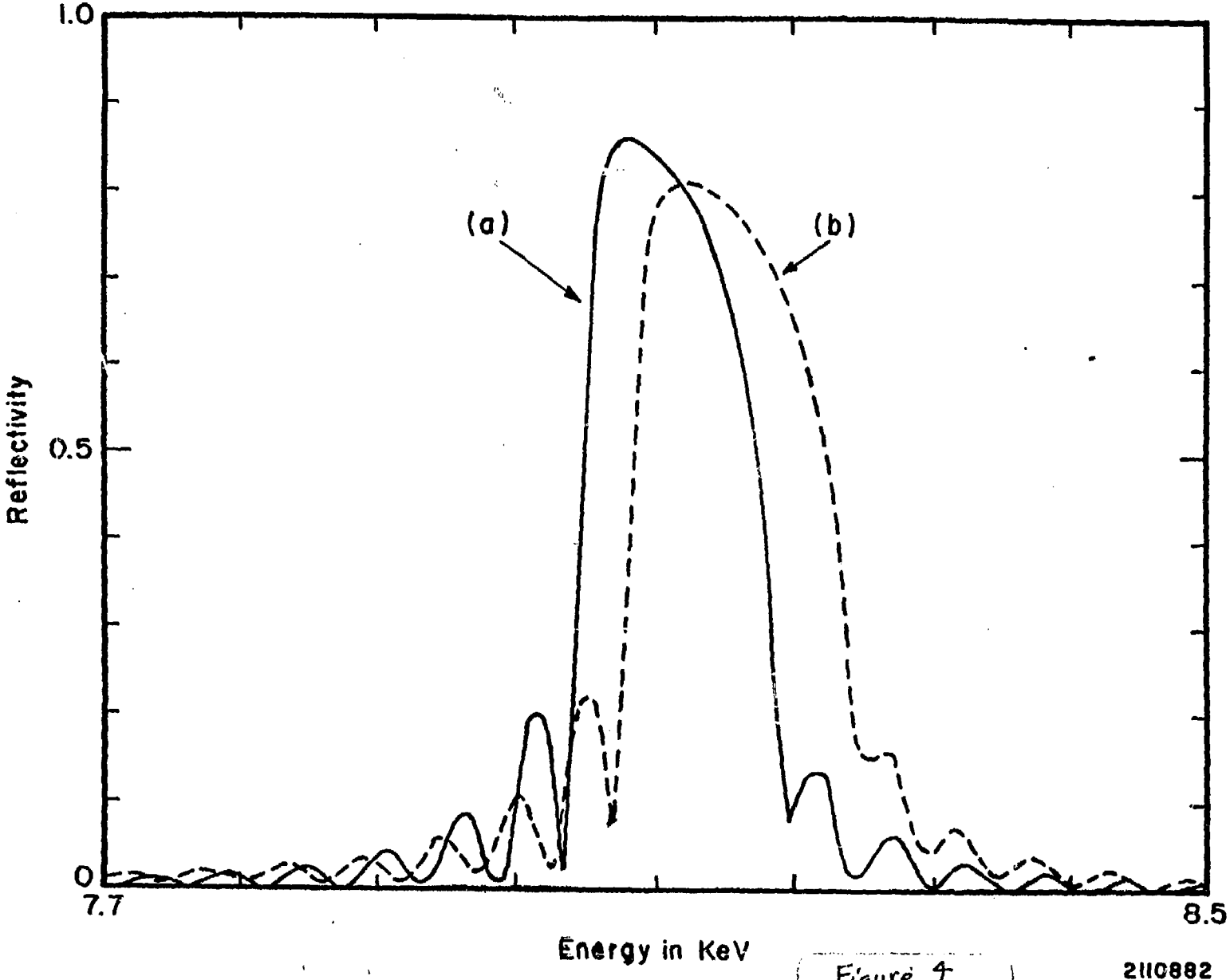

Figure 4
(a) ; (b)

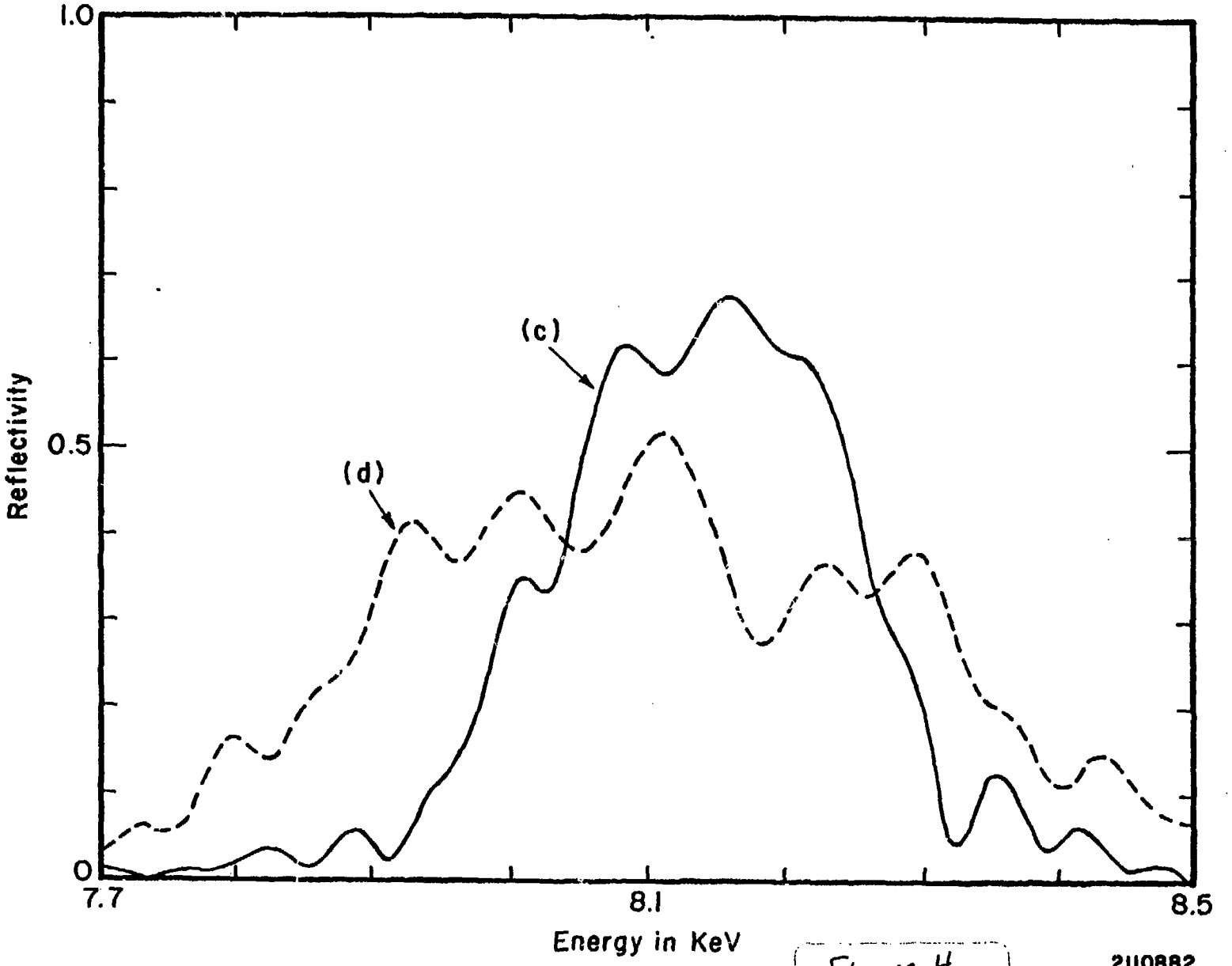

Figure 4
c, d

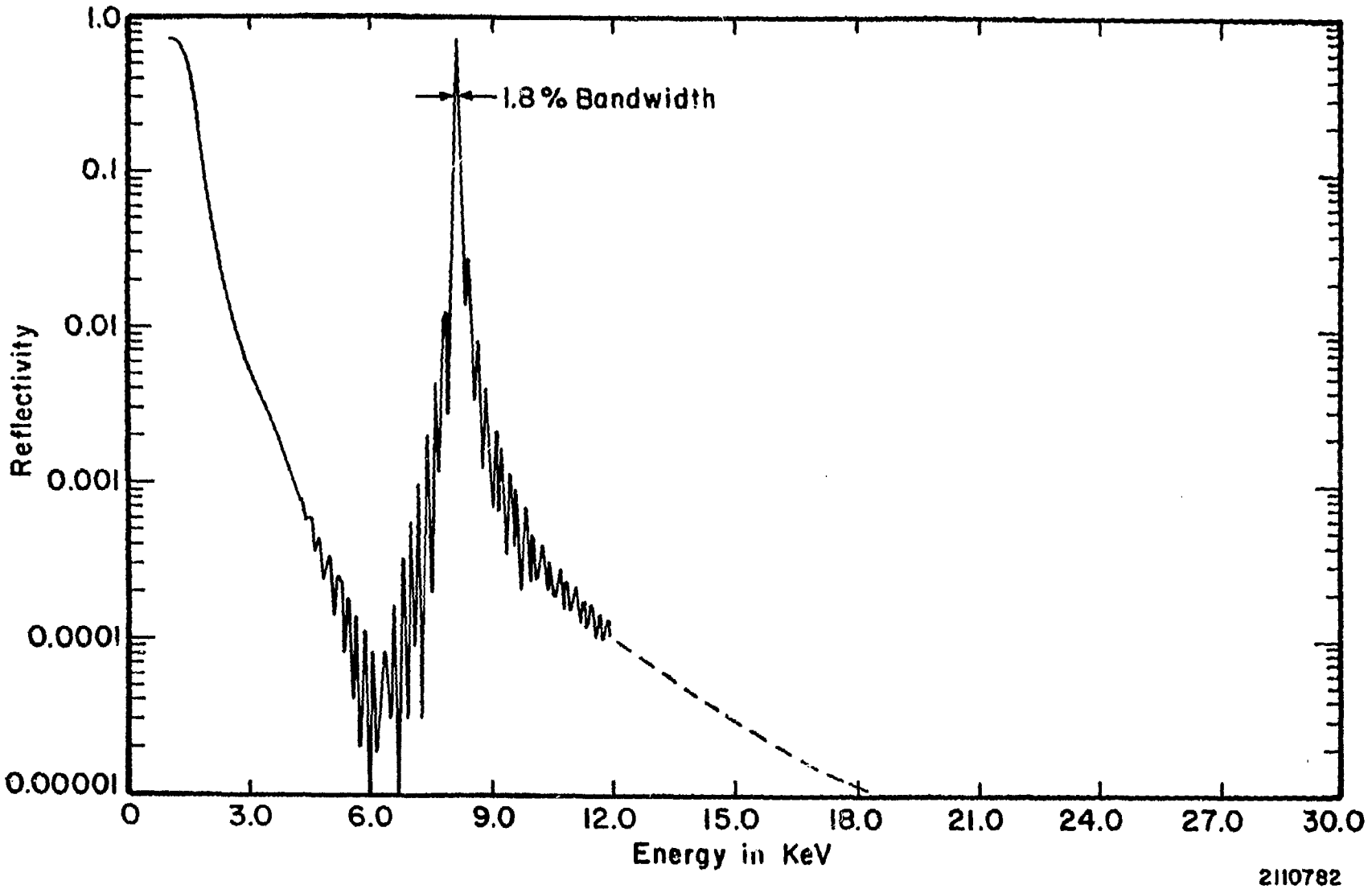
1.8% Bandwidth
Reflectivity
1.0
0.1
0.01
0.001
0.0001
0.00001
0
3.0
6.0
9.0
12.0
15.0
18.0
21.0
24.0
27.0
30.0
Energy in KeV
2110782

Figure 5

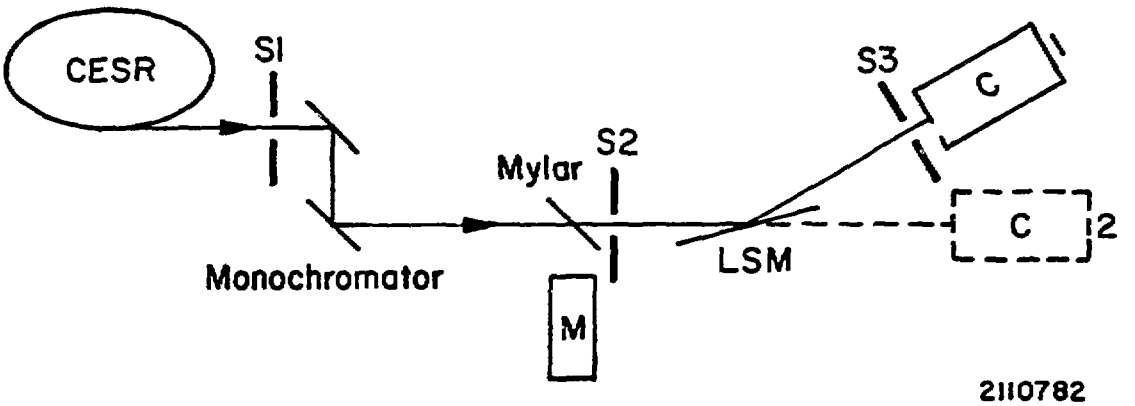

Figure 6

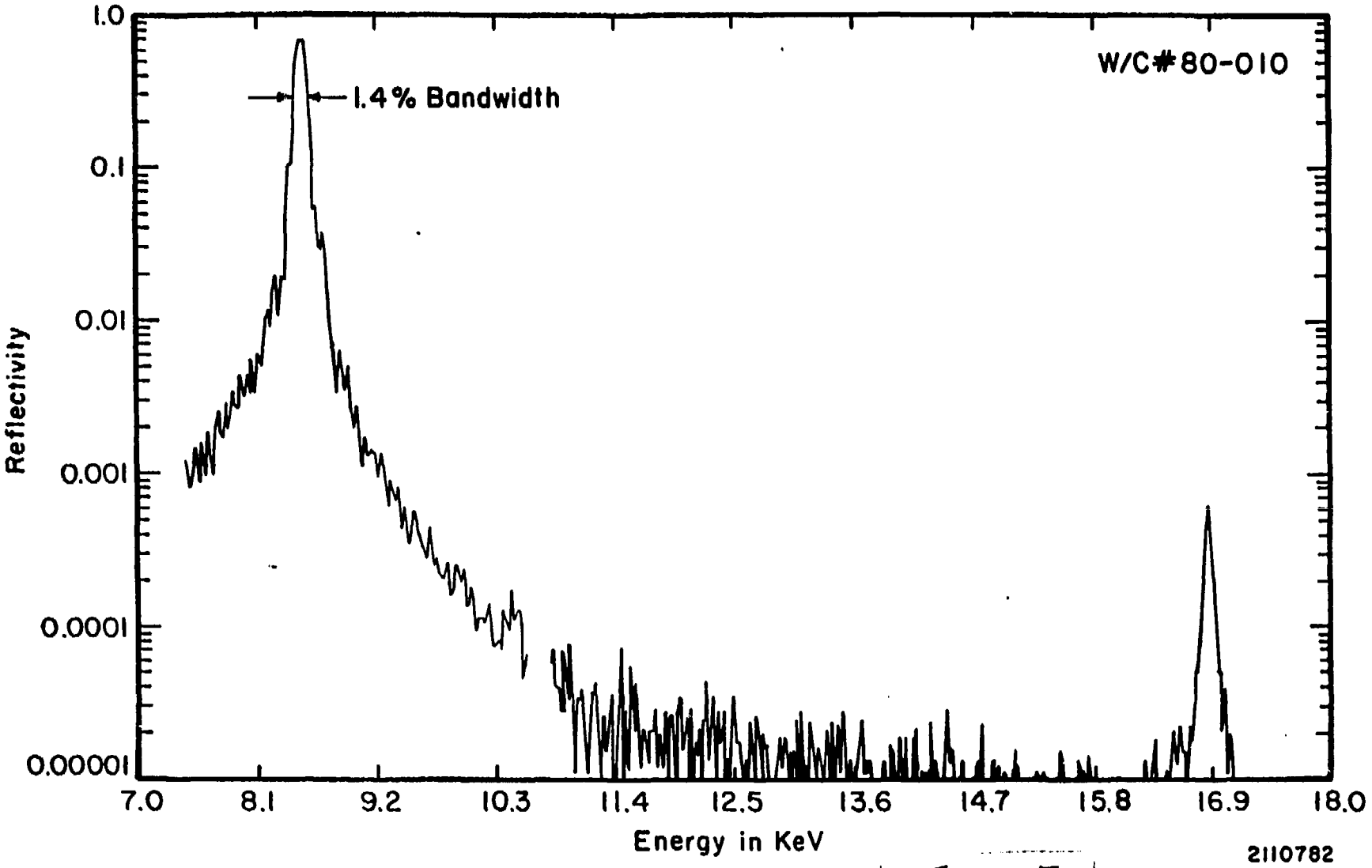
W/C#80-010
1.4% Bandwidth
Reflectivity
1.0
0.1
0.01
0.001
0.0001
0.00001
7.0
8.1
9.2
10.3
11.4
12.5
13.6
14.7
15.8
16.9
18.0
Energy in KeV
2110782

Figure 7

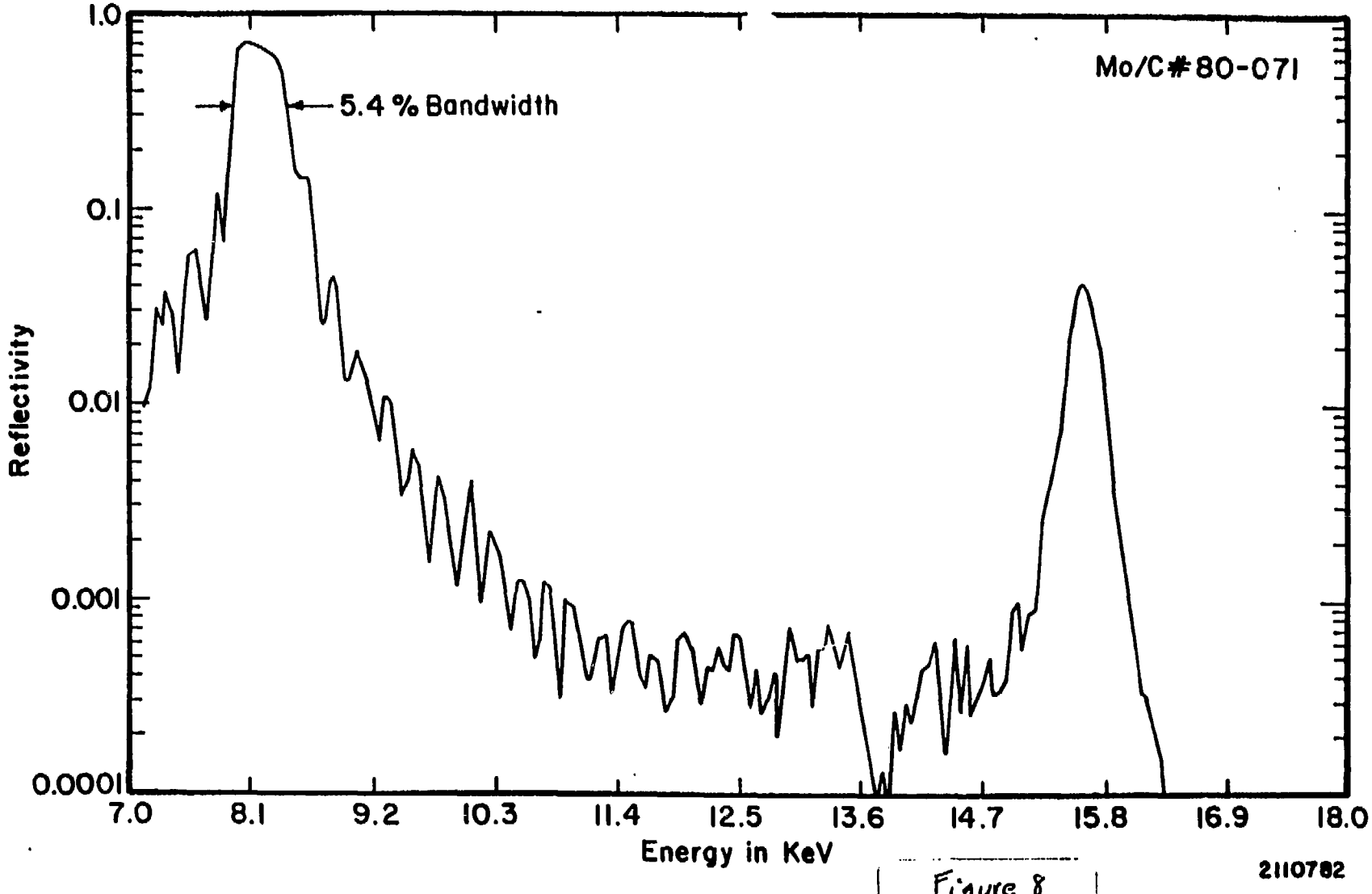
Mo/C#80-071
5.4 % Bandwidth
Reflectivity
1.0
0.1
0.01
0.001
0.0001
7.0
8.1
9.2
10.3
11.4
12.5
13.6
14.7
15.8
16.9
18.0
Energy in KeV
2110782

Figure 8

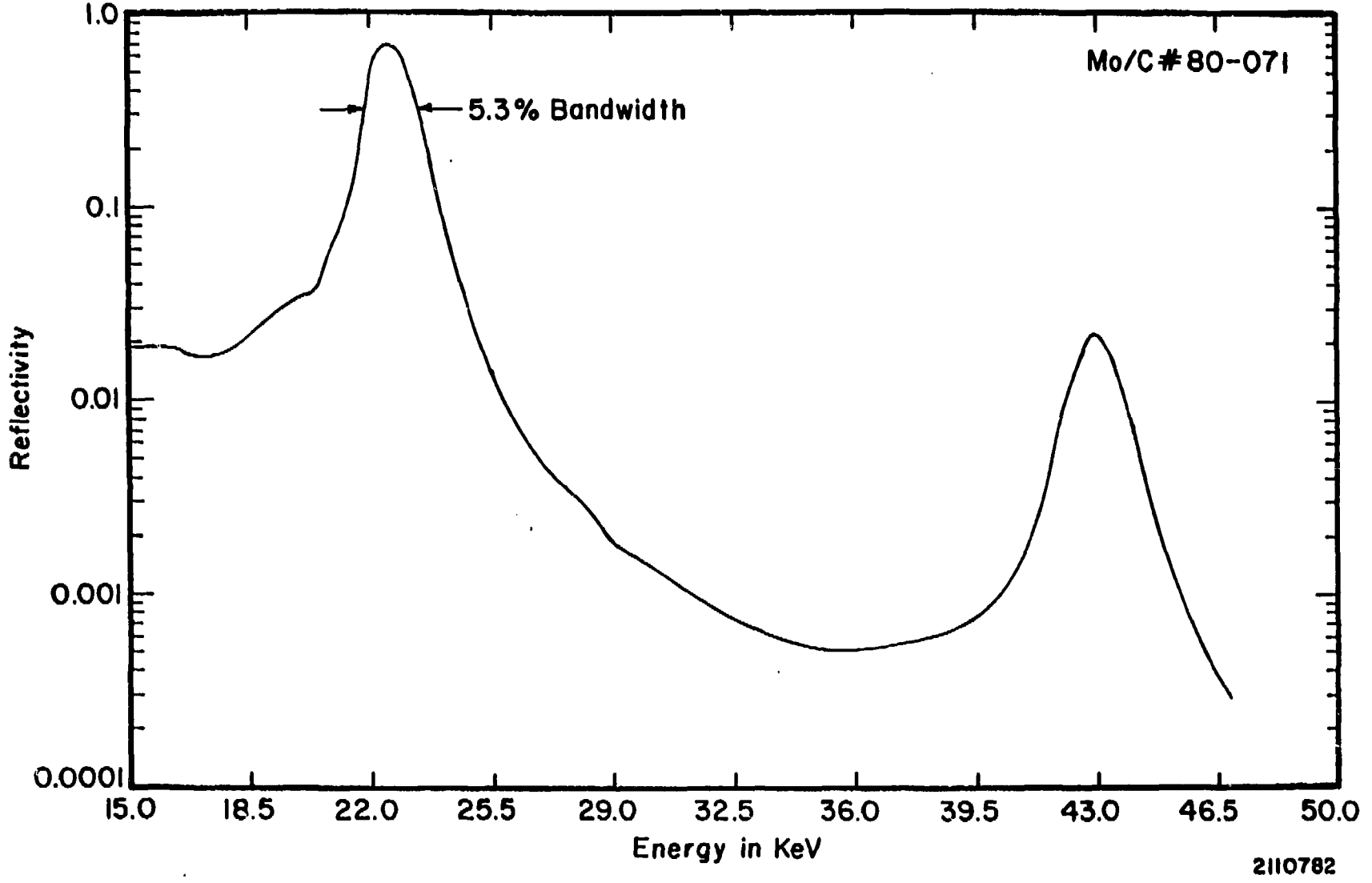
Mo/C #80-071
5.3% Bandwidth
Reflectivity
1.0
0.1
0.01
0.001
0.0001
15.0
18.5
22.0
25.5
29.0
32.5
36.0
39.5
43.0
46.5
50.0
Energy in KeV
2110782

Figure 9

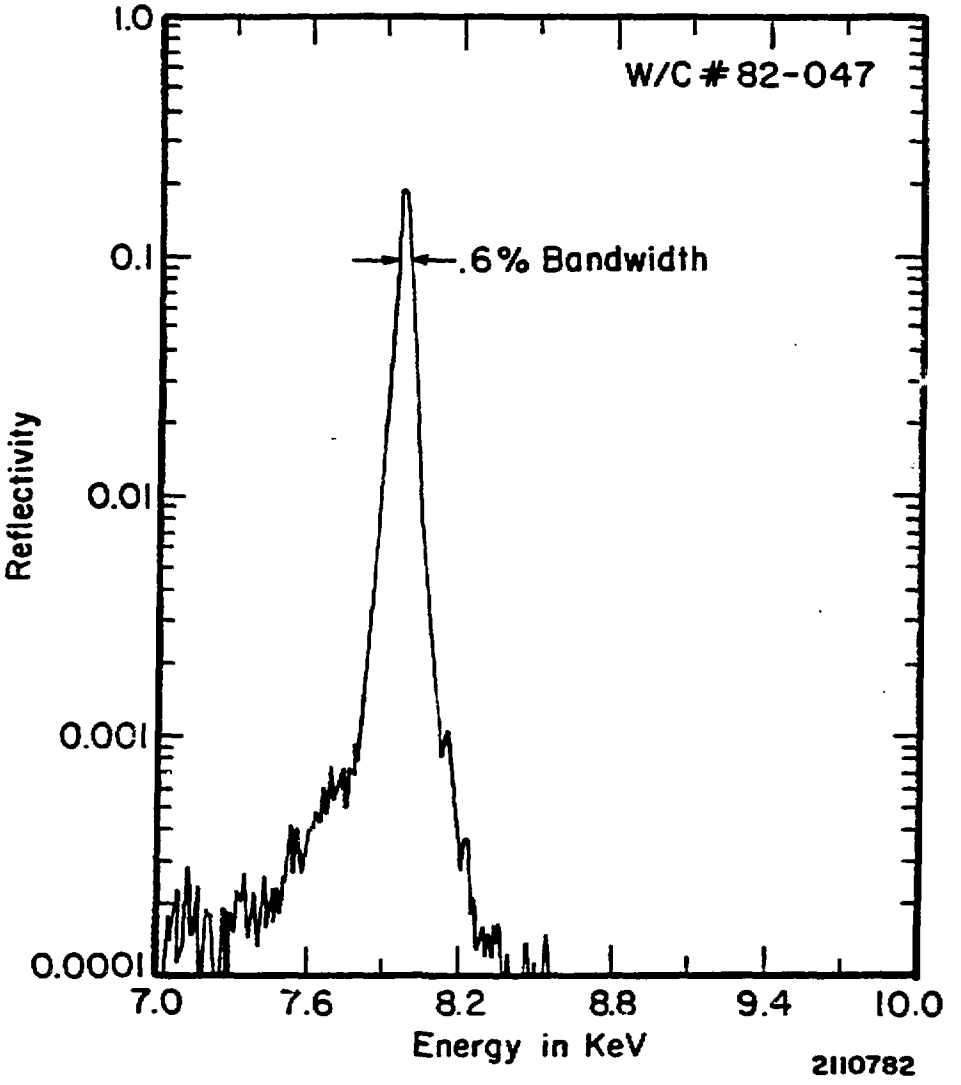
W/C # 82-047
.6% Bandwidth
Reflectivity
1.0
0.1
0.01
0.001
0.0001
7.0
7.6
8.2
8.8
9.4
10.0
Energy in KeV
2110782

Figure 10

Figore
11

ORNL-DWG 81-13501R2

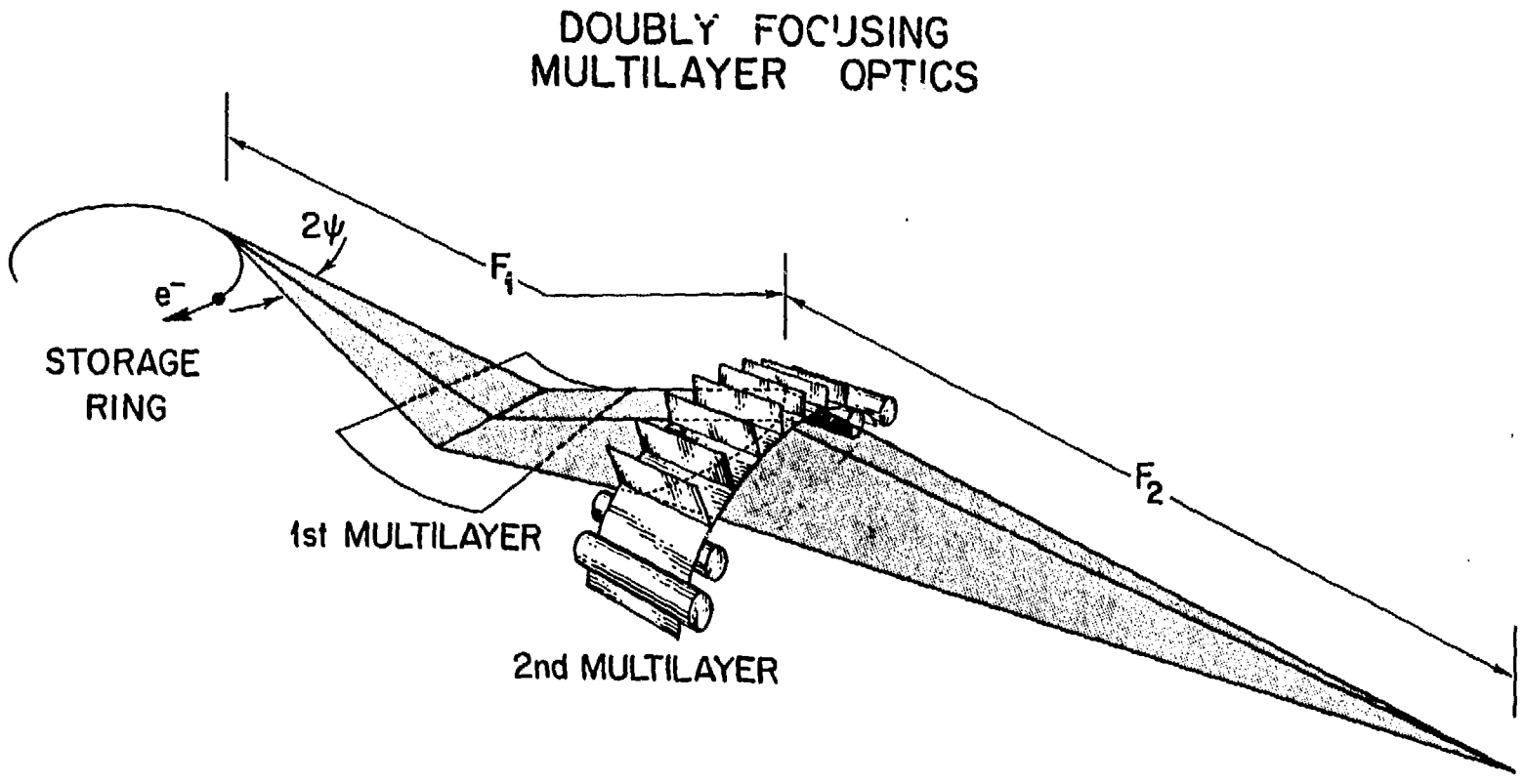

Figure
12

DISCLAIMER